MATHEMATICAL BIOSCIENCES
AND ENGINEERING
Volume **8**, Number **4**, October **2011**

doi:10.3934/mbe.2011.8.915

pp. **915–930**

A MATHEMATICAL MODEL OF THE PURKINJE-MUSCLE JUNCTIONS

Adnane Azzouzi, Yves Coudière and Rodolphe Turpault

Université de Nantes, Laboratoire de Mathématiques Jean Leray, Nantes, France

Nejib Zemzemi

Inria, Reo team, Rocquencourt, France

(Communicated by Yang Kuang)

Abstract. This paper is devoted to the construction of a mathematical model of the His-Purkinje tree and the Purkinje-Muscle Junctions (PMJ). A simple numerical scheme is proposed in order to perform some simple numerical experiments.

1. **Introduction.** The sequence of electrical activation of the human heart heavily relies on the coordination between several different excitable tissues. In normal conditions, the excitation of the ventricles is triggered by the depolarization of the atrio-ventricular (AV) node which propagates quickly through the His bundle and Purkinje fibers. This special conduction network is isolated from the muscle except at its endpoints that are connected to the ventricular wall at special sites called Purkinje-Muscle Junctions (PMJ). Modeling this network and its interaction with the muscle is therefore crucial to build realistic ventricle models.

In this article, we propose a mathematical formulation of a model of the His-Purkinje network and the PMJ. This problem has been addressed by several authors. We refer to [18] for a recent review. Many of these models were based on cellular automata approaches, like for example [3, 11, 15]. Such models are quite good at representing the macroscopic electrical behavior. However, they rely on simplified and phenomenological macroscopic assumptions on the spatio-temporal coupling between cells. On the other hand, modern models of the propagation of the electrical excitation, namely the monodomain or bidomain equations [14] are of different nature and take into account the microstructure of the tissue. In such a context the main issue is to properly write the interaction between the continuous models of the 3D muscle and the special conduction network that should be represented by a tree with 1D branches. Some authors recently proposed a procedure to couple the 3D bidomain equations in the ventricle to some 1D monodomain equations in the Purkinje fibers [19, 6]. In these papers, the coupling is written at the discrete level, considering some mesh vertices as individual cells and the PMJ as a conductance between these vertices and an endpoint of the Purkinje tree. Such a procedure does

2000 *Mathematics Subject Classification.* Primary: 35Q92; Secondary: 65M08, 92C99.

Key words and phrases. Purkinje-Muscle Junction, monodomain equations, finite volumes.

This work was supported by the Grant ANR 07-JCJC-0141. It was mainly achieved during the summer session of the Cemracs school in August 2009.

not provide a correct continuous model of the PMJ, missing for instance the scaling between the 1D current out of the Purkinje tree and the 3D current in the muscle.

Our main objective is to write a relevant model of the His-Purkinje tree and the Purkinje-Muscle Junctions. To access such an issue, the monodomain equations are written both in the 3D muscle and in the 1D branches of the Purkinje tree. The PMJ is then considered to be a volume inside the muscle which contains a given surface of Purkinje cells. Consequently only two continuous parameters are required to describe the PMJ: the surface of Purkinje cells per unit volume ratio and the conductance per unit surface of the PMJ.

In order to test our model we propose a numerical method to solve these equations. It consists of a finite element and finite volume discretization in space and a first order explicit-implicit time-stepping scheme. Additionally, some numerical examples are provided, in order to show that the model behaves as expected. The first test illustrates anterograde and retrograde propagation of the action potential through the PMJ. The second example depicts how it can be embedded into a more complex optimization procedure.

The mathematical equations are given in section 2 and the numerical details are explained in section 3. Section 4 is devoted to the numerical illustrations.

2. A mathematical model of the Purkinje-Muscle Junctions.

The most complete description of cardiac electricity is given by the bidomain equations. The bidomain model consists of the equations for the extracellular potential and the transmembrane potential. We refer to [14] for more detailed derivation of bidomain model and further discussions. Moreover, in the absence of applied currents, propagating action potential on the scale of human heart can be studied with a monodomain model. Muzikant et al. [10] have proved that monodomain model can be validated against the spread of action potential wavefronts, whereas bidomain models can be validated against measurement of tissue potentials. In this work, the monodomain model is considered for the numerical computations. This model consist of a non linear partial differential equation for the transmembrane potential V.

2.1. The monodomain equations for excitable tissues.

A sample cardiac tissue like the myocardium is represented by a 2D or 3D domain denoted by Ω. Although the most complete description of cardiac electrical activity is given by the bidomain equations, the monodomain equations are sufficient to represent accurately the spread of the action potential wavefronts in general [10, 13]. For a single homogeneous tissue, it consists of the non linear partial differential equation for the transmembrane potential V,

$$A\left(C\partial_t V + I_{\text{ion}}(V,w)\right) = \operatorname{div}\left(G\nabla V\right) \quad \text{in } \Omega, \tag{1}$$

for any $t > 0$, coupled to the ordinary differential equations

$$\partial_t w + g(V,w) = 0 \quad \text{in } \Omega. \tag{2}$$

The space and time are measured in cm and s and eq. (1) is written in $\mu\text{A/cm}^3$. The parameters A, C and G are described in table 1 (see [12]). The transmembrane current I_{ion} is computed as a function of the transmembrane voltage $V(t,x) \in \mathbb{R}$ and some cell state variables denoted by $w(t,x) \in \mathbb{R}^m$. The dynamics of these variables is described by the system of equations (2). From the point of view of electrophysiology, the state variables are basically voltage dependent gating variables

(dimensionless) describing the activity of the ionic channels through the membrane and some concentrations in mmol/l as detailed in section 2.4. An isolated tissue sample is modeled by the following boundary condition

$$G\nabla V \cdot \mathbf{n} = 0, \quad \text{on } \partial\Omega \tag{3}$$

where $\partial\Omega$ is the boundary of Ω and $\mathbf{n}$ is the unit normal to $\partial\Omega$ outward of Ω, see figure 1(a). The problem is supplemented with an initial condition on V and w:

$$V(0,x) = V_0(x), \quad w(0,x) = w_0(x) \quad \text{for } x \in \Omega. \tag{4}$$

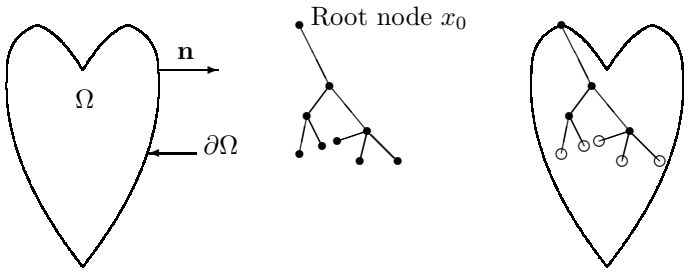

(a) Myocardium only.

(b) His-Purkinje tree only.

(c) Myocardium, conduction tree and Purkinje-Muscle Junctions.

FIGURE 1. Modeling framework.

A	Surface of membrane per unit volume	10^3cm^-1
C	Capacity per unit of surface	10^{-3}mF/cm^2
G	Average tissue conductivity	1mS/cm
V	Transmembrane voltage	-100 to 30mV
I_{ion}	Total membrane current per unit of surface	up to $300\mu\text{A/cm}^2$

TABLE 1. Average values of the parameters and their units

2.2. **The monodomain equations on a 1D network of excitable tissue.** The His bundle and Purkinje network is defined by a tree denoted by $H = (V, E)$ where $V = \{x_i,\ i = 0 \dots n\} \subset \mathbb{R}^d$ $(d = 2, 3)$ are its $n+1$ vertices and $E \subset \{(x, y) \in V \times V\}$ are its edges. This functional tree defines a subset of $\mathbb{R}^d$ still denoted by H and defined as the collection of the straight lines (x, y) for x and y vertices in V:

$$H = \bigcup_{e=(x,y)\in E} \{tx + (1-t)y,\ t \in (0,1)\}.$$

Note that straight lines were chosen for sake of simplicity. Any smooth path would be appropriate too. The tree is supposed to have $p+1$ endpoints numbered first and organized as follows : the root node is x_0 and the remaining endpoints are $\partial H = \{x_1, \dots x_p\}$, see figure 1(b). Note that $0 < p \leq n$.

Remark 1. The His-Purkinje network could be described more generally using a graph and assuming that each of its vertices is able to be coupled to the muscle or possibly excited by an external applied current (these conditions are not exclusive one from another). The case of a tree coupled through its endpoints only is described here for sake of simplicity.

It is natural to suppose that the propagation of the action potential through H follows the monodomain system of equations (1) and (2). But it needs to be specified since H is not an open subset in $\mathbb{R}^d$: equations (1) and (2) make sense as usual on each 1D edge $e = (x, y)$ in E, while the conservation of charges for an isolated domain H implies that Kirchhoff's law is written at each vertex of H. The unknown on the tree H is denoted by (V^H, w^H). It is a sequence of 1D unknown functions $V^H = (V_e)_{e\in E}$ and $w^H = (w_e)_{e\in E}$. These functions are solutions to eqs. (1) and (2) on each edge $e \in E$ and to Kirchhoff's law at all the vertices of H:

$$\forall x \in V, \quad \sum_{e\in E(x)} G_e(x)\nabla V_e(x)\cdot \mathbf{n}_e = 0 \tag{5}$$

where $E(x)$ is the set of all edges $e = (x, y)$ that share x as a common endpoint and $\mathbf{n}_e = (x - y)/|x - y|$ is the unit vector colinear to e outward of e at point x, see figure 2(a). On the boundary $\partial H = \{x_1, \dots x_p\}$ and the root node x_0 of the His-Purkinje tree, the set $E(x)$ contains only one edge and condition (5) degenerates into the Neumann boundary condition stated in eq. (3).

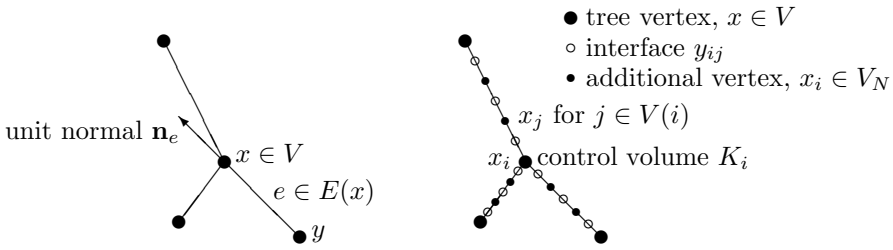

(a) Notations. (b) Mesh.

FIGURE 2. The His-Purkinje tree.

Similarly, the conductivity coefficient $G^H = (G_e)_{e\in E}$ is a sequence of 1D functions defined on the edges $e \in E$. *It can be discontinuous across edges* and the other parameters and functions are sequences of parameters and functions defined on the edges $e \in E$: $A^H = (A_e)_e$, $C^H = (C_e)$, $I^H_{\text{ion}} = (I_{\text{ion},e})$, $g^H = (g_e)$.

The theoretical existence and nature of solutions $V^H = (V_e)_{e\in E}$ and $w^H = (w_e)_{e\in E}$ is not investigated here. But it is assumed that such solutions are continuous on each vertex $x \in V$ so that it can be defined nodal values $V^H(x)$ for all $x \in V$.

2.3. **The Purkinje-Muscle Junctions.** It is important to note that the two electrophysiological problems modeled by the monodomain equations in the myocardium (from sec. 2.1) and the His-Purkinje network (from sec. 2.2) are uncoupled. One can solve for the action potential both in myocardium (either in 2D or 3D) and in the His-Purkinje network separately by solving the monodomain equation in both domains. The question of modeling the Purkinje-Muscle Junctions (PMJ) is now closely related to the question of coupling the 2D or 3D equations in the myocardium to the 1D monodomain equation in the His-Purkinje network.

It is a main objective of this paper to write such a 2D/1D or 3D/1D coupling condition. We assume that the coupling occurs through some Purkinje-Muscle Junctions (PMJ) localized at the endpoints $x_1, \dots x_p \in \partial H$ of the His-Purkinje tree H, while the root node x_0 is an excitation node (AV node for instance).

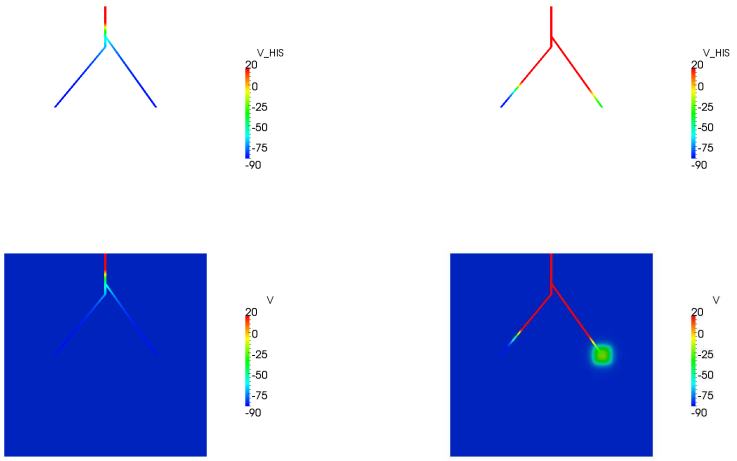

FIGURE 3. Example computation in a His-Purkinje tree coupled to a 2D slab of tissue.

The complex microstructure of the end of the Purkinje system and its actual coupling with the myocardium is hard to describe accurately [6, 1, 18]. The endpoints of the His-Purkinje tree are usually supposed to represent Purkinje cells and to be connected to several ventricular cells through some junctions, like in [6]. Here, a different interpretation is proposed. The tree equations from section 2.2 only model the His bundle and proximal Purkinje fibers, but not the extremal Purkinje fibers. Instead, the latter are supposed to spread out homogeneously into some volumetric regions around each endpoint $x_i \in \partial H$ of the His-Purkinje tree. Hence the junctions are not modeled individually but as a whole in these small regions. Therefore, it is associated to each endpoint x_i in ∂H a PMJ region denoted by $\Omega_i \subset \Omega$ with positive volume, $|\Omega_i| > 0$, see figure 1(c), that represents the volume into which the last Purkinje cells spread out from point x_i into the muscle. Let S_i denotes the surface of Purkinje fibers involved in such a junction and $e \in E$ denotes the edge to which x_i is an endpoint ($\{e\} = E(x_i)$), then the total current out of the His-Purkinje fiber at x_i is exactly

$$J_i = S_i \left(G_e(x_i) \nabla V_e(x_i) \cdot \mathbf{n}_i \right). \tag{6}$$

The average transmembrane potential of the Purkinje cells in the region Ω_i is $V_e(x_i)$.

On the other hand, the average transmembrane potential of the cardiomyocytes in the region Ω_i is

$$\langle V \rangle_i = \frac{1}{|\Omega_i|} \int_{\Omega_i} V(x) dx. \tag{7}$$

Following the idea that the PMJ acts as a conductance [6, 18], the coupling relation in region Ω_i reads

$$J_i = g_i \left(\langle V \rangle_i - V_e(x_i) \right) \tag{8}$$

where the coefficient g_i is the conductance of the Purkinje-Muscle junction number i (table 2). Given the transmembrane potential V in the muscle, this equation is a boundary condition for the monodomain system of equations in the Purkinje tree H. It replaces the Kirchhoff's law (3) on the endpoints $x_i \in \partial H$. On the other

S_i	surface of membrane of the Purkinje cells in Ω_i	cm^2
J_i	current from the Purkinje to the muscle in Ω_i	μA
s_i	volumetric source term function in Ω_i	$\mu\text{A}/\text{cm}^3$
$G_e(x_i)$	conductivity of the Purkinje fiber at endpoint x_i	mS/cm
g_i	conductance of the Purkinje-muscle junction in Ω_i	mS

TABLE 2. Units in the PMJ condition (8).

hand, the conservation of charges implies that a volumetric source term s_i is added to the monodomain equation in the muscle Ω. For the coupling region Ω_i, it reads

$$s_i(x) = \begin{cases} s_i := \frac{S_i}{|\Omega_i|} G_e(x_i)\nabla V_e(x_i)\cdot \mathbf{n}_i & \text{for } x \in \Omega_i, \\ 0 & \text{otherwise.} \end{cases} \tag{9}$$

Remark 2. Note that $\frac{S_i}{|\Omega_i|}$ is a surface to volume ratio, similar to the coefficient A in eq. (1). But it refers to the surface of PMJ per unit of muscle volume.

The system of equation that models a 2D/3D muscle Ω coupled to a 1D His-Purkinje tree $H = (V, E)$ finally reads:

$$A\left(C\partial_t V + I_{\text{ion}}(V,w)\right) + \sum_{i=1}^{p} s_i = \text{div}\left(G\nabla V\right) \quad \text{in } \Omega, \tag{10}$$

$$\partial_t w + g(V,w) = 0 \quad \text{in } \Omega, \tag{11}$$

$$G\nabla V\cdot \mathbf{n} = 0 \quad \text{on } \partial\Omega, \tag{12}$$

$$A_e\left(C_e\partial_t V_e + I_{\text{ion},e}(V_e,w_e)\right) = \text{div}\left(G_e\nabla V_e\right) \quad \text{on } e,\ \forall e \in E, \tag{13}$$

$$\partial_t w_e + g_e(V_e,w_e) = 0 \quad \text{on } e,\ \forall e \in E, \tag{14}$$

$$\sum_{e\in E(x)} G_e(x)\nabla V_e(x)\cdot \mathbf{n}_e = 0 \quad \forall x \in V\backslash\partial H, \tag{15}$$

$$G_e(x_i)V_e(x_i)\cdot \mathbf{n}_i = \frac{g_i}{S_i}\left(\langle V\rangle_i - V_e(x_i)\right) \quad i \in \{1,\dots p\} \tag{16}$$

where the source terms s_i are given by eq. (9). It is recalled that the parameters A, C, G are respectively the ratio of membrane of surface per unit volume, the capacitance and the conductivity coefficient in the media considered (table 1), while $I_{\text{ion}}(V,w) \in \mathbb{R}$ and $g(V,w) \in \mathbb{R}^m$ are nonlinear functions that describe the electrophysiology of the media.

For sake of simplicity, in the following applications, the values of the parameters A^H and C^H are assumed constant in space and the ionic model (the nonlinear functions I^H_{ion} and g^H) is the same all along the His-Purkinje tree, accounting for a tissue made of one singular cell type,

$$\forall e \in E, \quad A_e = A^H,\ C_e = C^H,\ I_{\text{ion},e} = I^H_{\text{ion}},\ g_e = g^H.$$

Only the conductivity coefficient $G^H = (G_e)_{e\in E}$ is assumed to vary along the His-Purkinje tree H.

Remark 3. The coupling is described by the data of the regions Ω_i $(i = 1\dots p)$ and by two numerical parameters, namely the junction's conductance per unit of surface, $\frac{g_i}{S_i}$ and the ratio of surface of Purkinje cells' membrane per unit volume of myocardium, $\frac{S_i}{\Omega_i}$.

2.4. **Physiological description of the ionic currents.** The equations from the Beeler & Reuter model [2] are used to compute the ionic currents $I_{\text{ion}}(V, w)$ in the muscle cells (so called BR model), while the equations from the DiFransesco & Noble model [8] are used to compute the ionic current $(I^H_{\text{ion}}(V^H, w^H))$ in the Purkinje cells (so called DFN model). Although there exists more up-to-date models for both Purkinje cells and ventricular cardiomyocytes [18], these simple representations are sufficient to model accurately enough and on a generic basis the spread of the action potential through the PMJ and its consequence on the sequence of activation of the muscle.

Hence, using the notations from the original paper [2] the unknowns w in the muscle Ω is specifically

$$w = (m, h, j, d, f, \xi_1, [Ca], i_{si}) \in \mathbb{R}^8$$

and the unknown w_e on each $e \in E$ is [8]

$$w_H = (y, x, r, m, h, d, f, f_2, p, [Ca]_i, [Ca]_{up}, [Ca]_{rel}, [K]_c, [K]_i, [Na]_i) \in \mathbb{R}^{15}.$$

The general structure of such a model is as follows:

- The variables w are split into $k > 0$ "gating variables" $(m, h, j, d, f, \xi_1$ for the BR model and $y, x, r, m, h, d, f, f_2, p$ for the DFN one) and $m - k \geq 0$ remaining ones, denoted respectively by $w_{\text{g}} \in \mathbb{R}^k$ and $w_r \in \mathbb{R}^{m-k}$;
- Each gating variable is solution of a quasilinear equation (see eq. (18));
- The remaining ones are given by a system of nonlinear equations;
- The current I_{ion} is computed as a function of the transmembrane potential V and $w = (w_{\text{g}}, w_r)$.

for the BR model, it reads:

$$C\frac{dV}{dt} = -I_{\text{ion}}(V, w) \tag{17}$$

$$\frac{dw_{\text{g}}}{dt} = \alpha(V, w_r)(1 - w_{\text{g}}) - \beta(V, w_r) \tag{18}$$

$$\frac{dw_r}{dt} = -g_r(V, w_{\text{g}}, w_r). \tag{19}$$

In these equations, α and β are diagonal matrices that does not depend on w_{g}.

The model for the His-Purkinje is similar, replacing C, V, w, w_{g}, w_r, α, β, I_{ion}, g_r by their counterparts C^H, V^H, w^H, w^H_{g}, w^H_r α^H, β^H, I^H_{ion}, g^H_r.

3. **Numerical method.** A finite element method will be used in the muscle domain Ω because it is well suited to parabolic type problems and a finite volume technique will be used in the His-Purkinje network H for its simplicity and ability to ensure Kirchhoff's law at each vertex $x \in V$ of the tree and the Robin boundary condition at its endpoints.

3.1. **Equations of the ventricular tissue.** Subsequently, the discretization in Ω requires a simplicial mesh $\mathcal{T}$ (triangles in 2D, tetrahedra in 3D) with N vertices, which is compatible with the geometry of the p coupling regions Ω_i, that is

$$\forall i = 1 \dots p, \quad \exists \mathcal{T}_i \subset \mathcal{T}, \quad \text{such that } \mathcal{T}_i \text{ is a simplicial mesh of } \Omega_i.$$

Lagrange Finite Elements of first order (see [7]) are used with a standard first order numerical quadrature. The discrete space is spanned by the N functions $(\phi_1, \dots \phi_N)$ and the nodal values of V and w are their coordinates with respect to this basis.

They are stored in vectors still denoted by $V = (V_1, \dots V_N)$ and $w = (w_1, \dots w_N)$. Hence eqs. (10) - (12) have the following semi-discrete discrete counterpart:

$$A\left(C\mathbf{M}\frac{dV}{dt} + \mathbf{M}I_{\text{ion}}(V,w)\right) + \mathbf{C}s = -\mathbf{K}V, \tag{20}$$

$$\frac{dw}{dt} + g(V,w) = 0. \tag{21}$$

In this system of equations, the vector $s = (s_1, \dots s_p)$ contains the value of the source terms in the p coupling regions as defined in equation (9) and the matrices $\mathbf{M}$ and $\mathbf{K}$ are the mass and stiffness matrices defined by

$$M_{ij} = \sum_{T\in\mathcal{T}} \frac{|T|}{d+1} \sum_{k=1}^{d+1} \phi_i(x_{i_k})\phi_j(x_{i_k}) \simeq \int_\Omega \phi_i(x)\phi_j(x)dx,$$

$$K_{ij} = \int_\Omega G(x)\nabla\phi_j(x)\cdot\nabla\phi_i(x)dx.$$

The mass matrix is diagonal due to the lumping arising from the quadrature formula and the stiffness matrix accounts for the boundary condition (12). Due to the numerical quadrature, the vectors $I_{\text{ion}}(V,w) = (I_{\text{ion}}(V_i,w_i))_{i=1\dots N}$ and $g(V,w) = (g(V_i,w_i))_{i=1\dots N}$ contain the nodal values of the nonlinear reaction terms I_{ion} and g. The approximation of the coupling source terms on line i of the system above reads

$$\sum_{j=1}^{p}\int_\Omega s_j(x)\phi_i(x)dx = \sum_{j=1}^{p} s_j \int_{\Omega_j}\phi_i(x)dx \simeq \sum_{j=1}^{p} C_{ij}s_j$$

$$\text{with } C_{ij} \simeq \int_{\Omega_j}\phi_i(x)dx = \sum_{T\in\mathcal{T}_j}\frac{|T|}{d+1}\sum_{k=1}^{d+1}\phi_i(x_{i_k}) \tag{22}$$

using again the numerical quadrature. The coefficients C_{ji} are the entries of the $N \times p$ coupling matrix $\mathbf{C}$.

3.2. **Computing the coupling terms.** The computation of the source term s_i involves the average values of the transmembrane potential V in the regions Ω_i which read

$$\langle V\rangle_i = \sum_{j=1}^{N} V_j \frac{1}{|\Omega_i|}\int_{\Omega_i}\phi_j(x)dx = \frac{1}{|\Omega_i|}\sum_{j=1}^{N} V_j C_{ji} = \frac{1}{|\Omega_i|}\left\{\mathbf{C}^T V\right\}_i.$$

where $\mathbf{C}$ is the $N \times p$ matrix defined in eq. (22).Hence, the source term s_i in region Ω_i reads

$$s_i = \frac{g_i}{S_i}\frac{S_i}{|\Omega_i|}\left(\frac{1}{|\Omega_i|}\left\{\mathbf{C}^T V\right\}_i - V_e(x_i)\right). \tag{23}$$

3.3. **Equations of the His-Purkinje tree.** Consider a set $V_N = \{x_1, \dots x_{N_H}\}$ of points in H that contains in particular all the vertices of H: $V \subset V_N$. Since H is a tree, the nodes from V_N define a set of M edges $E_M = \{e_j, j = 1 \dots M\}$ that are subsets of the original edges $e \in E$ as shown on fig. 2(b). This defines the tree (V_N, E_M) that is used to find a discrete solution for eqs. (13)-(16).

Therefore, consider the set $V_N(i) = (x_j)_j$ of the nodes in V_N that are connected to $x_i \in V_N$. In general, $\#V(i) = 2$ but the endpoints of H have $\#V(i) = 1$ and the

bifurcation nodes have $\#V(i) > 2$. It is associated to the node x_i a *control volume* K_i defined as

$$K_i = \cup_{j\in V_N(i)}[x_i, y_{ij}], \quad \text{where } y_{ij} = \frac{1}{2}(x_i + x_j) \text{ is the midpoint of } (x_i, x_j).$$

This control volume is a simple edge if $\#V(i) \leq 2$ and a star-shaped set (around x_i) if $\#V(i) > 2$, where Kirchhoff's law must be written. Note that x_i is not the midpoint of K_i in general.

Remark 4. The numbering of the nodes in the discrete graph (V_N, E_M) is supposed to be such that x_0 is the root node and $\{x_1, \dots x_p\}$ are still the endpoints of H, namely ∂H. Naturally, the numbering can always be changed to to follow this assumption.

The unknowns are functions piecewise constant V^H and w^H defined by their values $V^H = (V_i^H)_{i=1\dots N_H}$ and $w_e = (w_i^H)_{i=1\dots N_H}$ at the vertices $x_i \in V_N$. They are interpreted as average values of V^H and w^H on the control volumes K_i and the discretization is based on the integral formulation of eqs. (13)-(14) on the K_i. In view of Kirchhoff's law, the exact solution verifies, for the root node and any interior vertex $x_i \in V_N \backslash \partial H$,

$$\int_{K_i} A^H \left(C^H \partial_t V^H + I_{\text{ion}}^H(V^H, w^H)\right) dx = \sum_{j\in V_N(i)} G_e(y_{ij}) \nabla V^H(y_{ij}) \cdot \mathbf{n}_{ij}.$$

Here the index ij refers to the edge (x_i, x_j) that is a subset of edges $e \in E_M \subset E$. Assuming that V^H and w^H are functions piecewise constant on the K_i, the discretization reads, for $i = 1 \dots N_H$ (except for $x_i \in \partial H$):

$$A^H \left(C^H \frac{dV_i^H}{dt} + I_{\text{ion}}^H(V_i^H, w_i^H)\right) |K_i| = \sum_{j\in V_N(i)} F_{ij},$$

$$\frac{dw_i^H}{dt} + g^H(V_i^H, w_i^H) = 0$$

where $|K_i| = \sum_{j\in V_N(i)} |x_i - x_{ij}|$ is the measure of K_i and $F_{ij} \simeq \{G_e \nabla V^H \cdot \mathbf{n}_{ij}\}_{x=y_{ij}}$ approximates the flux of current out of K_i through the interface y_{ij} between K_i and K_j. The usual consistent finite difference approximation is used to compute this flux:

$$F_{ij} = G_e(y_{ij}) \frac{V_j^H - V_i^H}{d_{ij}} \quad \text{with } d_{ij} = |x_i - x_j|. \tag{24}$$

The numbers d_{ij} are the distances between the centers of K_i and K_j. Since the y_{ij} are the midpoints of the edges (x_i, x_j), the approximation of the flux is second order accurate and the measure of K_i reads $|K_i| = \frac{1}{2}\sum_{j\in V_N(i)} d_{ij}$.

For a boundary node $x_i \in \partial H$, the exact solution verifies

$$\int_{K_i} A^H \left(C^H \partial_t V^H + I_{\text{ion}}^H(V^H, w^H)\right) dx = \sum_{j\in V_N(i)} G_e(y_{ij}) \nabla V^H(y_{ij}) \cdot \mathbf{n}_{ij} + G_e(x_i) \nabla V^H(x_i) \cdot \mathbf{n}_i.$$

The last, additional, term is the flux of current outward of H. It has been replaced by its value according to the coupling relation from eq. (16).

At last, the approximation on the His-Purkinje tree reads, for all $i = 1 \dots N_H$,

$$A^H \left(C^H \frac{dV_i^H}{dt} + I_{\text{ion}}^H(V_i^H, w_i^H) \right) |K_i| = \sum_{j \in V_N(i)} F_{ij} + \underbrace{\frac{g_i}{S_i} \left(\langle V \rangle_i - V_i^H \right)}_{\text{only if } x_i \in \partial H},$$

$$\frac{dw_i^H}{dt} + g^H(V_i^H, w_i^H) = 0,$$

where the discrete flux F_{ij} are computed according to eq. (24).

At last, the approximation in the His-Purkinje tree can be written in matrix form as follows:

$$A^H \left(C^H \mathbf{M}_H \frac{dV^H}{dt} + \mathbf{M}_H I_{\text{ion}}^H(V^H, w^H) \right) = -(\mathbf{K}_H + \mathbf{G}_H) V^H + \mathbf{G}_H \, \text{diag}(|\Omega_i|^{-1}, 0) \mathbf{C}^T V, \tag{25}$$

$$\frac{dw^H}{dt} + g^H(V^H, w^H) = 0 \tag{26}$$

where $\mathbf{M}_H$ is a diagonal mass matrix, $\mathbf{K}_H$ is a stiffness matrix that discretizes the Homogeneous Neuman diffusion problem (both are $N_H \times N_H$ matrices); $\mathbf{G}_H$ is a $N_H \times N_H$ diagonal matrix of conductivities per unit of surface and $\text{diag}(|\Omega_i|^{-1}, 0)$ is a $N_H \times p$ diagonal matrix:

$$\mathbf{M}_{H\,ij} = |K_i| \delta_{ij}, \quad \mathbf{K}_{H\,ij} = \begin{cases} -\frac{G_e(y_{ij})}{d_{ij}} & \text{if } j \in V_N(i), \\ \sum_{j \in V_N(i)} \frac{G_e(y_{ij})}{d_{ij}} & \text{if } i = j, \\ 0 & \text{otherwise} \end{cases}$$

and

$$\mathbf{G}_H = \begin{pmatrix} \frac{g_1}{S_1} & & & \\ & \ddots & & \\ & & \frac{g_p}{S_p} & \\ & & & 0 \end{pmatrix}, \quad \text{diag}(|\Omega_i|^{-1}, 0) = \begin{pmatrix} \frac{1}{|\Omega_1|} & & & \\ & \ddots & & \\ & & & \frac{1}{|\Omega_p|} \\ 0 & \dots & 0 & \end{pmatrix}.$$

3.4. **Time discretization.** The semi-discrete problem is the nonlinear system of ordinary differential equations (20) and (21) with source term defined by eq. (23) together with equations (25) and (26).

For sake of numerical stability, the system should be discretized implicitly. Anyway, because of the complexity of the ionic models (functions I_{ion}, g and I_{ion}^H, g^H) an implicit-explicit strategy is used:

- the semilinear equations (18) on the gating variables are solved implicitly while the equations (19) are solved explicitly;
- the linear diffusion terms are solved implicitly.

Our first order discrete scheme is as follows:

$$A\left(C\mathbf{M}\frac{V^{n+1}-V^n}{\Delta t}+\mathbf{M}I_{\text{ion}}(V^n,w^{n+1})\right)+\mathbf{C}s^n=-\mathbf{K}V^{n+1}, \tag{27}$$

$$\frac{w_{\text{g}}^{n+1}-w_{\text{g}}^n}{\Delta t}=\alpha(V^n,w_r^n)(1-w_{\text{g}}^{n+1})-\beta(V^n,w_r^n)w_{\text{g}}^{n+1}, \tag{28}$$

$$\frac{w_r^{n+1}-w_r^n}{\Delta t}=-g_r(V^n,w_{\text{g}}^{n+1},w_r^n), \tag{29}$$

$$\begin{aligned}A^H\left(C^H\mathbf{M}_H\frac{V^{H,n+1}-V^{H,n}}{\Delta t}+\mathbf{M}_H I_{\text{ion}}^H(V^{H,n},w^{H,n+1})\right)\\ =-(\mathbf{K}_H+\mathbf{G}_H)V^{H,n+1}+\mathbf{G}_H\,\text{diag}(|\Omega_i|^{-1},0)\mathbf{C}^TV^n,\end{aligned} \tag{30}$$

$$\frac{w_{\text{g}}^{H,n+1}-w_{\text{g}}^{H,n}}{\Delta t}=\alpha^H(V^{H,n},w_r^{H,n})(1-w_{\text{g}}^{H,n+1})-\beta(V^{H,n},w_r^{H,n})w_{\text{g}}^{H,n+1}, \tag{31}$$

$$\frac{w_r^{H,n+1}-w_r^{H,n}}{\Delta t}=-g_r(V^{H,n},w_{\text{g}}^{H,n+1},w_r^{H,n}), \tag{32}$$

$$s_i^n=\frac{g_i}{S_i}\frac{S_i}{|\Omega_i|}\left(\frac{1}{|\Omega_i|}\left\{\mathbf{C}^TV^n\right\}_i-V_i^{H,n}\right),\quad i=1\dots p. \tag{33}$$

The numerical algorithm at each time step is:

1. update the gating variables by solving the implicit linear equations (28) and (31);
2. update the ionic concentrations using equations (29) and (32);
3. Compute $I_{\text{ion}}(V^n,w^{n+1})$, $I_{\text{ion}}^H(V^{H,n},w^{H,n+1})$ and the coupling variables s_i^n according to equation (33);
4. Update both transmembrane potentials using equations (27) and (30).

4. Numerical experiment.

4.1. **Direct coupled problem.** In this paragraph we provide simulations of the Purkinje-muscle junctions in a normal case. In fact, by simplifying the problem, we suppose that the myocardium is coupled to the His bundle only in two different regions. Figure 4 shows the propagation of the action potential after it starts by external stimulation on the top of the His bundle: the wave starts at point x_0, the depolarization wavefront propagates along the His network towards the coupling regions. The left region is activated slightly earlier than the right one because the length of the right His bundle branch is slightly shorter than the left one. Once the coupling regions are activated, the action potential wave front propagates further in the myocardium. The model parameters are reported in table 3.

Parameter	His/Purkinje	Ventricle
$A(\text{cm}^{-1})$	500	500
$C(\text{mF/cm}^2)$	0.001	0.001
$G(\text{mS/cm})$	300	3

Coupling parameter	Value
$\frac{S_i}{\lvert\Omega_i\rvert}(\text{cm}^{-1})$	500
$\frac{g_i}{S_i}(\text{mS/cm}^2)$	300

TABLE 3. Monodomain parameters

In order to simulate a pathological case like a right bundle branch block (RBBB), the conductivity of the right branch of the His bundle is set to zero. Therefore the myocardium is only activated in the left coupling region, as shown on figure 5:

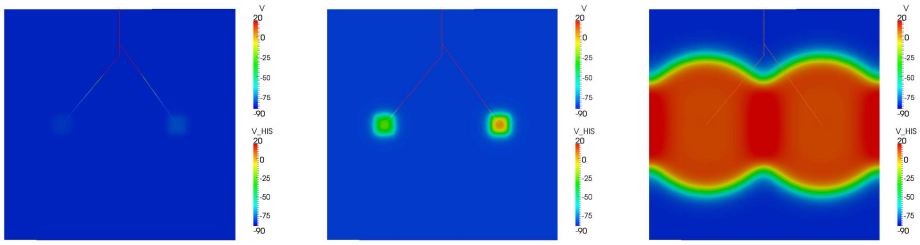

(a) 1.6ms (b) 2.0ms (c) 7.0ms

FIGURE 4. A normal activation of the His bundle brunches: snapshots of the action potential in the His bundle and the myocardium.

compared to the normal condition simulation, the activation of the right side of the muscle is delayed.

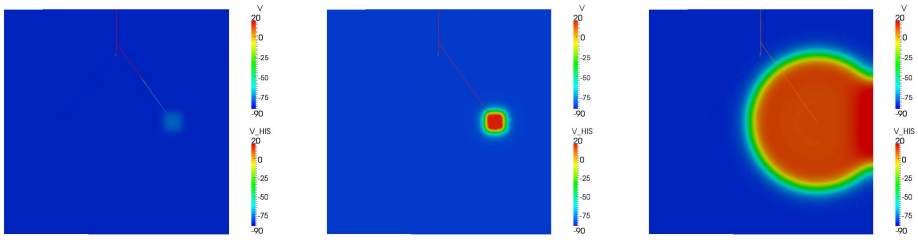

(a) 1.6ms (b) 2.0ms (c) 7.0ms

FIGURE 5. A Right bundle brunch block: snapshots of the action potential in the His bundle and the myocardium.

In the next paragraph we present the pacing technique as a tool to improve the depolarization time of the whole muscle.

4.2. **Optimized sites of stimulation for a RBBB.** The pacemaker is an electrical device which provides small electrical shocks to the heart muscle in order to regulate its beating. Many of today's pacemakers have two main components which are the electrodes and the transducer. The electrodes are implanted in the heart and allow to conduct the current from the medical device to the heart wall. The transducer is a small battery that generates the electrical discharge at a pre-determined frequency. Transducers deliver an electrical shock only when the heart is pacing too slow: it can therefore adapt the frequency of the electrical stimulation to the patient situation. On the contrary, the position of the pacemaker electrode is fixed once for all during the surgical intervention. Hence, the choice of the pacemaker position is crucial and have to be carefully determined before starting the surgical operation. A wrong placement can introduce serious problems [16, 17] and a second operation could be necessary to change the position of the pacemaker or to remove it.

The coupled model described in previous sections is now used on an simple academic test case to investigate how to optimize the position of the electrode. The

model of the electrode, the cost function and optimization algorithm are introduced in the next paragraph. Numerical results are then shown.

4.2.1. *pacemaker model.* The main role of heart electrical pacing in a RBBB condition is to minimize the delay of activation between the two ventricles. In our study the pacemaker is modeled using three parameters: the geometry of the probe, the amplitude of the stimulation current and its frequency. The contact between the pacemaker electrode and the myocardium is supposed to occur in a ball $B(x_p, r_p) = \{y \in \Omega, \quad |y - x_p| < r_p\}$, where x_p defines the position of the pacemaker center and r_p is the radius of the contact ball. The pacemaker is assumed to stimulate the myocardium once per cardiac cycle. Let T_p denotes the duration of each stimulation. The pacemaker is represented by a time-dependent external applied current, so that equation (10) is replaced by

$$A\left(C\partial_t V + I_{\text{ion}}(V,w)\right) + \sum_{i=1}^{p} s_i + I_p(x_p, T_p) = \text{div}\left(G\nabla V\right) \quad \text{in } \Omega. \tag{34}$$

The function $I_p(x_p, T_p)$ is given by

$$I_p(x_p,T_p)_{x,t} = \begin{cases} I_0 & \text{if } x \in B(x_p,r_p) \text{ and } \cos\left(\frac{\pi T_p}{T}\right) \leq \cos\left(\frac{\pi(2t-T_p)}{T}\right) \leq 1, \\ 0 & \text{otherwise.} \end{cases}$$

where I_0 is the amplitude of the stimulation and T denotes the duration of the cardiac cycle. Since they are related to the transducer modeling, the amplitude I_0 and the period T_p of the pacemaker are supposed to be fixed and positive constant. The different parameters used to define the pacemaker stimulation are given in table 4.

T_p	Pacing duration	2.0 ms
r_p	Radius of the pacemaker	1.5 mm
I_0	Value of the pacing current	$7.1\mu\text{A/cm}^3$
T	Cardiac cycle	700.0 ms

TABLE 4. Values of the parameters defining the pacemaker current.

In order to optimize the position of the electrode, we choose to maximize the number of depolarized cells at time T_d when the whole heart would be depolarized in normal conditions. Hence, T_d basically represents the length of the QRS complex. The depolarization threshold is set to $V_{th} = 0\,\text{mV}$. Given $x \in \Omega$ the position of the electrode, the region of interest is then defined by its measure:

$$M(x) = \left|\{y \in \Omega,\ V(T_d, y) > V_{th}\}\right|.$$

The minimization problem

$$\text{find } x_p \in \Omega, \quad J(x_p) = \min_{x\in\Omega} J(x), \quad J(x) = 1 - \frac{M(x)}{|\Omega|} \tag{35}$$

is a natural candidate to solve our problem.

Any solution of this problem involves the lagrangian defined by:

$$L(x,\Lambda) = J(x) - \Lambda \cdot g(x)$$

where $\Lambda = (\lambda_i)_i$ is the vector of the Lagrange multipliers and $g = (g_i)_i$ is the function of the inequality constraints $g_i(x) \leq 0$. If $x^\star$ is a solution of the problem (35) then there exists $\Lambda^\star$ such that the Kuhn-Tucker conditions are satisfied, namely:

$$\nabla J(x^\star) + \sum_i \lambda_i^\star \nabla g_i(x^\star) = 0$$

$$\forall i, \quad g_i(x^\star) \leq 0, \ \lambda_i^\star \geq 0, \quad g_i(x^\star)\lambda_i^\star = 0.$$

Generally a gradient descent method is used to find $x^\star$. In order to avoid the computation of the gradient ∇J and since our constraints are linear (see next paragraph), the algorithm *active set* will be used. It relies on a finite difference approximation of this gradient [9]. For practical reasons we used the `fmincon` function from MATLAB's optimisation toolbox. Additionally this function is also able to handle nonlinear constraints.

4.2.2. *Results.* In this paragraph we report an example showing how cardiac pacing could resynchronize the electrical activity of the heart. In order to emphasize the role of the pacing technique on the cardiac resynchronization, we have performed a RBBB pathological case by considering zero conductivity in the right branch of the His bundle as described in section §4.1. Our goal is to find the optimal position of the pacemaker probe allowing to maximize the volume of tissue that is depolarized at time T_d. To reach this aim we use the function cost and the algorithm described in section §4.2. The results are reported in Figure 6: in the first (respectively second, respectively third) column we present snapshots of RBBB (respectively normal, respectively pacing) case at different times. Comparing the RBBB simulation (first column) to the normal simulation (second column), we remark a clear asynchrony between the left and the right parts in the RBBB case. In particular at time T_d (11.8 ms), the entire myocardium is depolarized in the normal case whereas in the pathological case, an important region in the right part is not yet depolarized. That is responsible of an increasing of the QRS-complex duration in case of ECGs simulations [5, 4]. This delay between the right and the lefts parts of the myocardium depolarization has been significantly reduced when using the pacing technique. In particular at time T_d, one can see that the whole ventricle is almost depolarized. In this simulation, the initial placement of the probe was in the left bottom corner of the square. The same result was obtained when taking as initial position the right bottom corner.

5. **Discussion.** Up to now, existing models of the PMJ were not fully satisfactory from a mathematical point of view. The main objective of this paper is to give a well-posed mathematical framework to model the PMJ which can easily be discretized in order to simulate the interaction between the His-Purkinje network and the muscle. Our model given by eqs. (10)-(16) fulfills this objective. Since it is completely written from the continuous level, it is fully independent of the mesh. Furthermore, only two physical parameters are required to describe it, namely the surface of Purkinje cells per unit volume ratio $\frac{S_i}{|\Omega_i|}$ and the conductance per unit surface of the PMJ $\frac{g_i}{S_i}$. A natural and standard numerical scheme has proved to be efficient enough to perform some simple experiments.

For sake of simplicity, we present only 2D numerical examples although the model is developed for 3D applications. The only additional difficulty arising in 3D is purely technical. The objective was not to present realistic simulations but simple tests to illustrate the robustness of the model. Performing more realistic

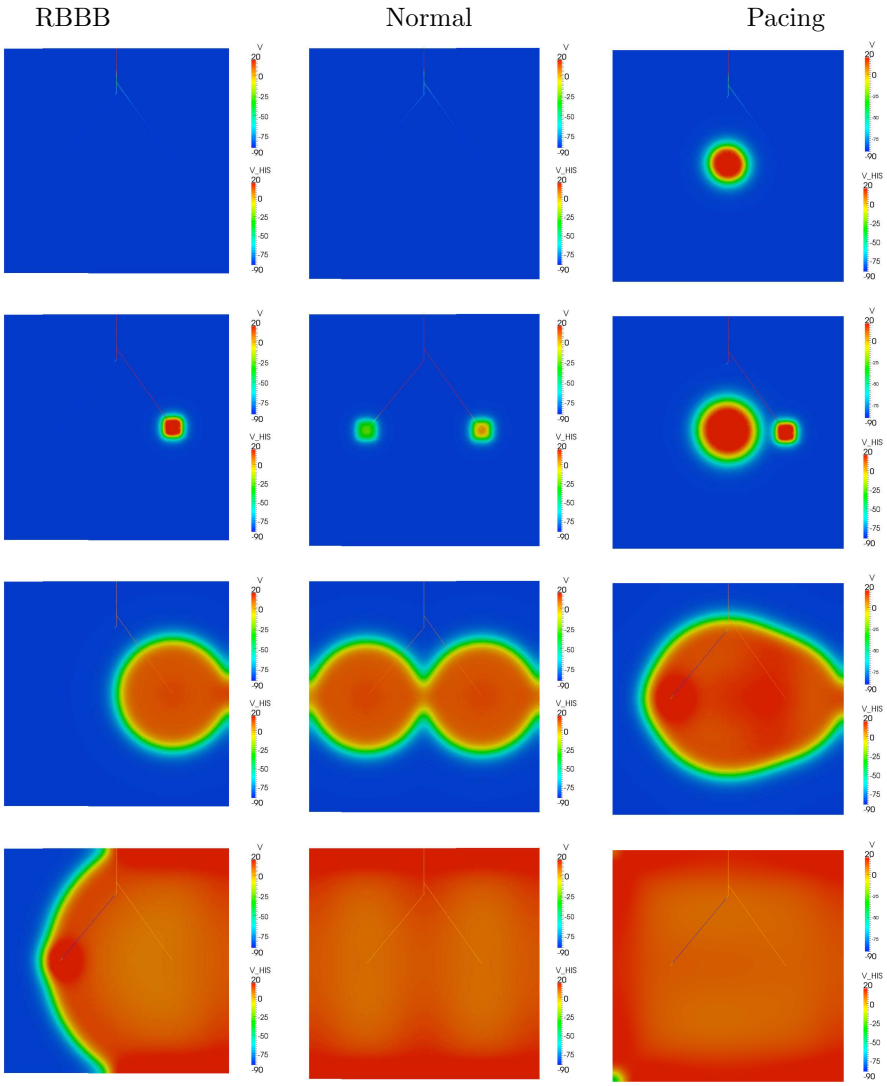

FIGURE 6. Comparison of the action potential propagation between RBBB, normal and a paced RBBB condition: Snapshots at times (from top to bottom) 1.0 ms, 2.0 ms, 6.0 ms and 11.8 ms.

simulations would require to take into account the geometry of the ventricle and to integrate the fast conduction network into it. Moreover, our first choice of the coupling parameters gives irrealistic PMJ delays in the anterograde and retrograde propagation. Therefore they need to be improved. These two points are beyond the scope of this work.

An additional improvement of the model would be to consider surfacic PMJ instead of volumic ones in order to better represent the behavior of the human heart.

REFERENCES

[1] A. V. Aslanidi, P. Stewart, M. R. Boyett and H. Zhang, *Optimal velocity and safety of discontinuous conduction through the heterogeneous purkinje-ventricular junction*, Biophysical Journal, 2009.

[2] G. Beeler and H. Reuter. *Reconstruction of the action potential of ventricular myocardial fibres*, J. Physiol. (Lond.), **268** (1977), 177–210.

[3] O. Berenfeld and J. Jalife, *Purkinje-muscle rentry as a mechanism of polymorphic ventricular arrhytmias in a 3-dimensional model of the ventricles*, Circ. Res., **82** (1998), 1063–1077.

[4] M. Boulakia, S. Cazeau, M. A. Fernández, J. F. Gerbeau and N. Zemzemi, *Mathematical modeling of electrocardiograms: A numerical study*, Annals of Biomedical Engineering, **38** (2010), 1071–1097.

[5] M. Boulakia, M. A. Fernández, J.-F. Gerbeau and N. Zemzemi, *Towards the numerical simulation of electrocardiograms*, in "Functional Imaging and Modeling of the Heart" (eds. F. B. Sachse and G. Seemann), Lecture Notes in Computer Science, Springer-Verlag, (2007), 240–249.

[6] P. M. Boyle, M. Deo, G. Plank and E. J. Vigmond, *Purkinje-mdeiated effects in the response of quiescent ventricles to defibrillation shocks*, Annals of Biomedical Engineering, 2009.

[7] P. G. Ciarlet, "The Finite Element Method for Elliptic Problems," North-Holland, 1978.

[8] D. DiFrancesco and D. Noble, *A model of cardiac electrical activity incorporating ionic pumps and concentration changes*, Phil. Trans. R. Soc. Lond., **307** (1985), 353–398.

[9] Philip E. Gill, Walter Murray and Margaret H. Wright, "Practical Optimization," Academic Press Inc., Harcourt Brace Jovanovich Publishers, London, 1981.

[10] C. S. Henriquez, A. L. Muzikant and C.K. Smoak, *Anisotropy, fiber curvature, and bath loading effects on activation in thin and thick cardiac tissue preparations: Simulations in a three-dimensional bidomain model*, Journal of Cardiovascular Electrophysiology, **7** (1996), 424–44.

[11] B. Milan Horacek, K. Simelius, R. Hren and J. Nenonen, *Challenges in modelling human heart's total excitation*, in "Functional Imaging and Modeling of the Heart," LNCS, (2001), 39–46.

[12] J. Keener and J. Sneyd, "Mathematical Physiology," Springer, New York, 1998.

[13] M. Potse, B. Dube, J. Richer, A. Vinet and R. M. Gulrajani, *A comparison of monodomain and bidomain reaction-diffusion models for action potential propagation in the human heart*, IEEE Transactions on Biomedical Engineering, 2006.

[14] J. C. Neu and W. Krassowska, *Homogenization of syncytial tissues*, Crit. Rev. Biomed. Eng., **21** (1993), 137–199.

[15] A. E. Pollard and R. C. Barr, *The construction of an anatomically based model of the human ventricular conduction system*, IEEE Transaction on Biomedical Engineering, **37** (1990), 1173–1185.

[16] W. B. Ross, S. M. Mohiuddin, T. Pagano and D. Hughes, *Malposition of a transvenous cardiac electrode associated with amaurosis fugax*, Pacing and Clinical Electrophysiology, **6** (1983), 119–123.

[17] W. A. Schiavone, L. O. N. W. Castle, E. Salcedo and R. Graor, *Amaurosis fugax in a patient with a left ventricular endocardial pacemaker*, Pacing and Clinical Electrophysiology, **7** (1984), 288–292.

[18] K. H. W. J. Ten Tusscher and A. V. Panfilov, *Modelling of the ventricular conduction system,* Progress in Biophysics and Molecular Biology, 2008.

[19] E. J. Vigmond and C. Clements, *Construction of a computer model to investigate sawtooth efects in the purkinje system,* IEEE Transaction on Biomedical Engineering, **54** (2007).

Received October 8, 2010; Accepted May 2, 2011.

E-mail address: adnane.azzouzi@univ-nantes.fr
E-mail address: yves.coudiere@univ-nantes.fr
E-mail address: rodolphe.turpault@univ-nantes.fr
E-mail address: nejib.zemzemi@comlab.ox.ac.uk